Environmental Science and Pollution Research (2019) 26:25550–25563
https://doi.org/10.1007/s11356-019-05851-2

RESEARCH ARTICLE

Nano-sized Prussian blue immobilized costless agro-industrial waste for the removal of cesium-137 ions

Ahmed Mohamed Shahr El-Din[1] · Tarek Monir[1] · Moubarak A. Sayed[2]

Received: 4 April 2019 / Accepted: 24 June 2019 / Published online: 2 July 2019

Abstract

For human health and safety, it is of great importance to develop innovative materials with a vast capacity for powerful removal of radioactive ions from aqueous solutions. Prussian blue functionalized sugarcane bagasse (PB-SCB) was successfully prepared for the efficient elimination of radioactive cesium (^{137}Cs) using a nontoxic, environmentally friendly, and costless method. The prepared renewable material was characterized using different techniques to emphasize morphology, functional groups, crystal structure, and the adsorption process. The adsorption of Cs(I) was better fitted to the pseudo-second-order model than pseudo-first-order model which revealed a chemical adsorption mechanism. The experimental isotherm results were best illustrated by the Freundlich model ($R^2 = 0.98$). Besides, the obtained values for the thermodynamic parameters indicating that the adsorption process was endothermic and spontaneous in nature. In addition to demonstrating high adsorption capacity for Cs ion removal (56.7 mg/g at 30 °C), PB-SCB might consider being an efficient and cost-effective adsorbent for the decontamination of cesium, where an estimated cost analysis revealed that the expenditure for the removal of 1000 mg/L cesium from alkaline radioactive wastewater is likely to be US$0.12.

Keywords Radioactive cesium · Prussian blue · Bagasse · Adsorption

Introduction

One of the most suspicious components of nuclear fallout and radioactive liquid waste is the radioactive cesium and especially ^{137}Cs due to its long half-life (30 years), high energy gamma-ray emission, high water solubility (Calarese 2011), and high transport abilities, which can be dissolved in soils and finally ending to be absorbed by plants, animals, and human (Ding and Kanatzidis 2010). In addition, its biological behaviors analogous to that of K^+ have been stated to be responsible for many problems leading to cancer, genetic mutation, genetic disorders, and others (Wang et al. 2019). Moreover, the critical nuclear accidents occurred in 1986 in Chernobyl (Russia) (Ming-hua et al. 1988), in 1987 in Goiania (Brazil) (Oliveira et al. 1991), and in 2011 at the Fukushima Daiichi nuclear power station (Manolopoulou et al. 2011), caused a severe release of huge amounts of ^{137}Cs which is a very hazardous radionuclide from the environmental standpoint.

Therefore, the decontamination of the radioactive species from the environment and the decommissioning of the old power plants (Neroda et al. 2014) are essential requirements for the efficient management of liquid wastes in the nuclear industry.

In this respect, numerous methods have been developed for the removal of cesium from radioactive liquid waste, such as chemical precipitation, evaporation, adsorption, membrane separation, liquid-liquid extraction, ion exchange, and biological methods (Attallah et al. 2009; Borai et al. 2008).

Highlights
- PB-SCB nano-adsorbent was facilely synthesized by a simple eco-friendly method.
- PB-SCB exhibited a maximum adsorption capacity of 56.7 mg/g for Cs removal from radioactive liquid waste.
- The Cs^+ adsorption by PB-SCB was governed by both chemisorption and physisorption mechanisms.
- PB-SCB demonstrated enhanced adsorption toward cesium in the presence of competing cations.

Responsible editor: Tito Roberto Cadaval Jr

✉ Ahmed Mohamed Shahr El-Din
ashahreldin@yahoo.com; ahmed.shahreldin@eaea.org.eg

[1] Hot Lab. Center, Atomic Energy Authority, Cairo 13759, Egypt

[2] Central Lab. for Elemental and Isotopic Analysis, Atomic Energy Authoritys, Cairo 13759, Egypt

According to various previous studies, Prussian blue (PB) have the ability for the selective adsorption of the alkali cations, particularly cesium ions (Sangvanich et al. 2010), in which PB is a dark-blue pigment, with the formula $Fe_7(CN)_{18}$ and a crystal cage size similar to the hydration radius of Cs^+ (Thammawong et al. 2013). The micro- or nano-size of PB ion-exchanger requires complex filtration or centrifugation systems, and to improve the practical application of it, it might be helpful to immobilize the particles in or at the surface of a support material (Vincent et al. 2014), as a binding matrix for providing a mass transfer unit that can be applied for field applications (Vincent et al. 2015). For example, PB particles were bound to the nonwoven fabric as a carrier (Vipin et al. 2013). The PB particles were also embedded in calcium/alginate beads (Mihara et al. 2016), in polyarylacetylene resin (Yang et al. 2015), in chitosan sponge (Parajuli et al. 2016), or in inorganic binders (Kawamoto et al. 2012).

Agricultural waste materials are of special attention as they are contained some of the natural polymers, including cellulose (50%), polyoses (27%), and lignin (23%) (Yu et al. 2017b). These polymers make them rich in hydroxyl, phenolic, and carbonyl groups which are expected to interact with heavy metal ions (Li et al. 2017) over a wide range of pH (up to 12) (Noor et al. 2017). Of particular concern in agriculture wastes is the sugarcane bagasse (SCB) (Bagasse is the fibrous residue left over after squeezing sugarcane for its juice and as a by-product from the bioethanol and sugar mills).

To the best of our knowledge, there is no work yet in the literature for the incorporation of PB onto bagasse as a costless agro-industrial waste for the adsorption of cesium ions. Furthermore, large capacity is still the objective for the successful treatment of cesium waste.

Herein, this study presents an efficacious procedure to synthesize functionalized Prussian blue adsorbent for highly effective removal of cesium ions from alkaline solutions by a one-pot, room-temperature method.

Experimental

Materials

All chemicals used during this study were analytically pure and used as supplied without further purification. $FeCl_3 \cdot 6H_2O$ and potassium hexacyanoferrate ($K_3[Fe(CN)_6]$) were purchased from Sigma-Aldrich, and cesium chloride (CsCl) salt from Fluka Company. The radioisotope sample of ^{137}Cs was obtained from the second Egyptian Research Reactor.

Preparation of PB-SCB hybrid adsorbent

No-cost, locally available, eco-friendly SCB was collected, washed thoroughly with tap water to remove dust, and then boiled in water for 1 h to remove the sweet materials. Subsequently, before sun-dried, the obtained SCB was rinsed with deionized water and milled to 0.125 mm. The PB-SCB hybrid was synthesized through in situ co-precipitation method as reported elsewhere with some modifications (Alamudy and Cho 2018). In this method, 4 g of bagasse was added to 25 mL of 0.062 M $K_4[Fe(CN)_6]$ solution under magnetic stirring. Then, 25 mL of 0.082 M $Fe(NO_3)_3 \cdot 9H_2O$ solution was introduced to the previous mixture with adjusting the solution pH at 2 using hydrochloric acid (0.1 M). The solution was kept stirring overnight at room temperature. Before the obtained blue colored material subjected to air drying, it was filtered and washed until the washing liquor was colorless (Figs. 1 and 2).

Adsorbent characterization and instrumentation

The prepared PB-SCB adsorbent morphologies were visualized by scanning electron microscopy (SEM; JXA-840A; JEOL; Japan). To recognize the functional groups, the structures of the samples were recorded by Fourier transform infrared spectroscopy (FT-IR, Nicolet spectrometer, Meslo, USA). An X-ray diffraction pattern of PB-SCB nanoparticles was measured using CuKα radiation by Schimadzo X-ray diffractometer, and the sample was scanned for 2θ ranging from 2 to 55.

Atomic absorption spectrometry (AAS, Varian AA20 spectrometer) was used for the measurement of inactive Cs^+ ion concentration in which the samples were collected, filtrated, and analyzed. The radiometric analysis of the cesium radioisotope (^{137}Cs) in the real sample solution was done using multichannel NaI (Tl) scintillation detector (model 3M3/3-X, Canberra Industries Inc., USA).

Determination of point of zero charge

The point of zero charge (pH_{Pzc}) was estimated following the procedure reported by Igberase and Osifo (2015). In this context, after adjusting the pH values of 5 ml (0.1 M) NaCl series in the range (2–10) (pH initial) using NaOH and HCl (0.1 M each), equal amounts (0.03 g) of PB-SCB were separately added to these solutions. These mixtures were agitated at room temperature for 24 h. Then, the solutions were filtered and pH of the filtrates was determined (pH final). By plotting the difference between initial pH_i and final pH_f, ($\Delta pH = pH_f - pH_i$), against the pH_i, the point of intersection at which ΔpH = zero is called the point of zero charge. The same procedure was applied for the determination of SCB point of zero charge.

Fig. 1 Digital image for the preparation of PB-SCB adsorbent

Adsorption experiments

Sorption of inactive cesium

The batch technique was applied to evaluate the applicability of the PB-SCB adsorbent to remove Cs^+ ions from alkaline solutions. For safety precautions, during the batch technique, inactive cesium was chosen as a model ion for radiocesium, since they have similar chemical behaviors in the aqueous solutions (Yu et al. 2017a). In this respect, different effective parameters such as pH (2–12) and contact time (5 min-6 h) were examined by mixing 0.01 g of the prepared adsorbent with 5 ml of Cs^+ (50 mg/L). For isotherm studies, cesium solutions having different initial concentrations (25–300 mg/L) were exposed to a fixed quantity of the PB-SCB (2 g/L) at predetermined equilibrium time (3 h) at different temperatures (303–333 K). The prepared adsorbent weight parameter was carried out in the range of (5–20) mg. The interfering ion influence on the adsorption of Cs^+ ion was investigated utilizing various concentrations of Li^+, Na^+, and K^+ in the range (25–100 mg/L). The removal efficiency (% R) and the adsorption capacities at any time t (q_t, mg/g) and at equilibrium (q_e, mg/g) retained on the PB-SCB adsorbent were calculated in addition to the distribution coefficient (K_d) using the following equations respectively:

$$\%R = [(C_o - C_e)/C_o] \times 100 \quad (1)$$

$$q_e = (C_o - C_e) \times \frac{V}{m} \text{ (mg/g)} \quad (2)$$

$$qt = (C_o - C_t) \times \frac{V}{m} \text{ (mg/g)} \quad (3)$$

$$K_d = [(C_o - C_e)/C_o] \times \boldsymbol{V/m} \quad (4)$$

where C_o, C_e, and C_t are the initial, equilibrium concentration, and concentration at any time t of the metal ions, respectively, in the aqueous solution (mg/L); m is the adsorbent mass (g), and V is the solution volume (L); while V in the case of K_d (ml/g) is in milliliters.

Application on LLRLW sample

Static study

Low-level radioactive liquid waste (LLRLW) sample contains ^{137}Cs (140×10^3) Bq/L produced from the second Egyptian Research Reactor was subjected to the adsorption process with the prepared PB–SCB adsorbent where the effect of PB-SCB weight (10, 50) mg on the decontamination factor (DF) at different time intervals was calculated by the following equation:

$$DF = A_o/A_e \quad (5)$$

where (A_o) and (A_e) are the initial and final activities (Bq/ml) of the real radioactive Cs(I) samples, respectively, after treatment with PB-SCB adsorbent. All the previous experimental work was repeated two times (duplicated) to avoid the exposure to radioactive ^{137}Cs.

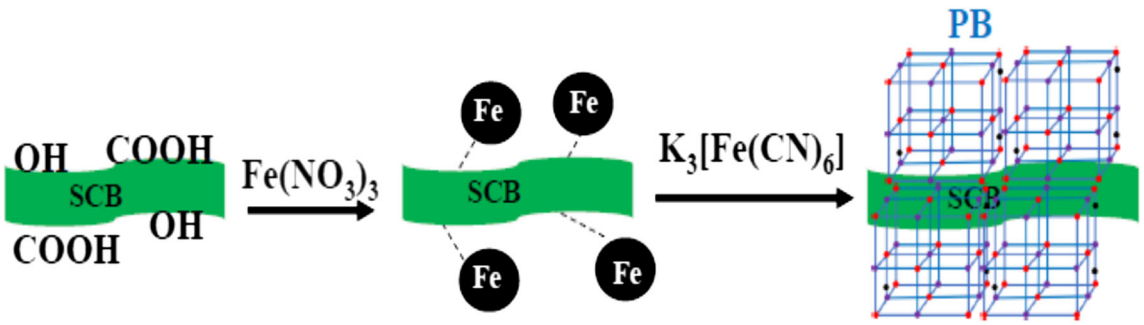

Fig. 2 Scheme for the preparation of PB-SCB adsorbent

Dynamic study

Column experiment was performed to investigate the dynamic removal of real radiocesium solution through adsorption. Total 0.25 g of PB-SCB was packed in a glass column with a length of 100 mm and an internal diameter of 6.5 mm. The radiocesium solution (50 ml) of total activity (7000 Bq) was pumped downward through the top of the column at a flow rate of 2.5 ml/min. Effluent samples were gathered from the column exit at regular time intervals and then analyzed for residual activity in the total 50 ml radioactive wastewater solution.

Result and discussion

Characterization of the samples

The obtained morphology given in Fig. 3a, b showed that the smooth surface, sheet-like structure SCB is retained after impregnation with PB (Su et al. 2018). The X-ray diffractogram obtained from the unmodified SCB and the PB decorated SCB is shown in Fig. 3c. The diffraction patterns revealed that 5 new characteristic peaks correspond to 17.364, 22.294, 24.523, 35.197, and 39.57 can be clearly assigned to the successful anchoring of PB on the surface of SCB which is consistent with other reports (Jang and Lee 2016; Chang et al. 2018). The FT-IR analysis illustrated in Fig. 3d confirms the signature of PB with the absorption vibration band at 2086 Cm^{-1} which corresponds to the C≡N group (Basu et al. 2018). Peaks that appear at 3700, 3400, 1719, and 1400 on the PB-SCB FTIR spectrum are attributed to the stretching vibration bands for OH (from COOH), OH (from H_2O), C–H (from CH_2 in cellulose), C=O (from ketone and aldehyde), and C=C (from aromatic rings), respectively. The 1050 Cm^{-1} band ascribed for C–O bending. It can be inferred from the FTIR spectrums for both SCB and PB-SCB that C=O might take part in the functionalization process, where the band of CO shifted from 1730 to 1719 Cm^{-1}.

SCB and PB-SCB point of zero charge determination

Point of zero charge (pH_{Pzc}) is the point at which the surface texture charge of an adsorbent is zero. When a solution pH surpasses this point, the surface of an adsorbent will be negative; therefore, the adsorption efficiency for cations will be

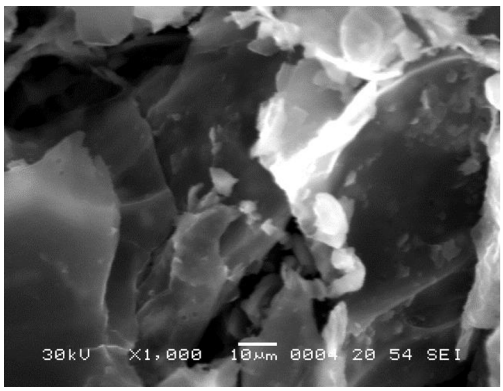

(a) SEM image of SCB

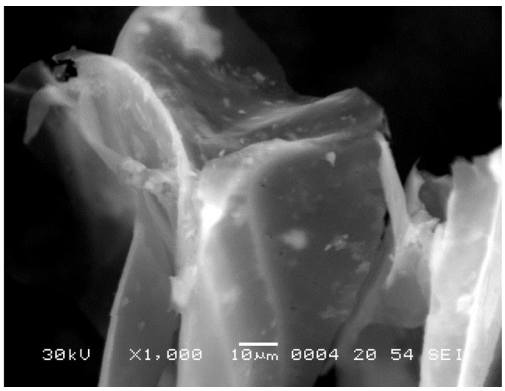

(b) SEM imageof PB-SCB adsorbent

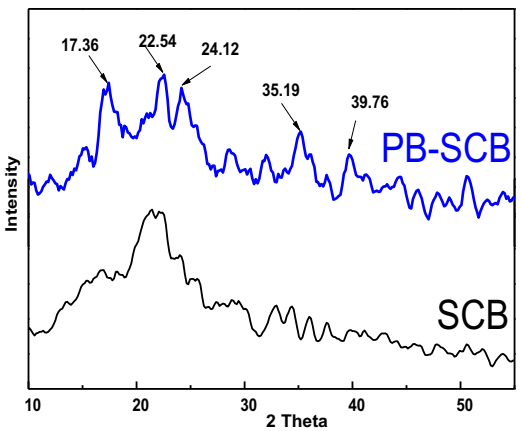

(c) XRD patternof SCB, PB-SCB adsorbent

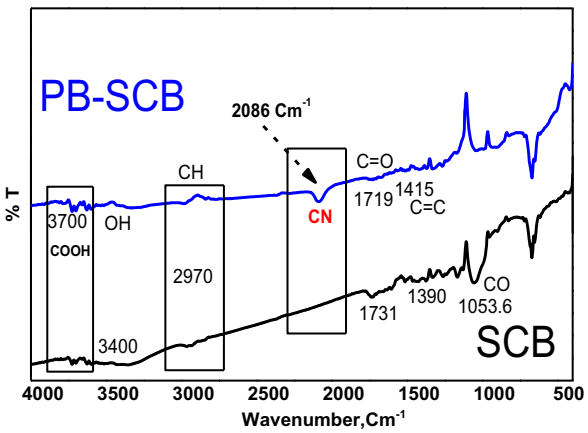

(d) FT-IR spectrum for SCB, PB-SCB adsorbent

Fig. 3 Characterization of SCB and PB-SCB adsorbent: (**a**) SEM image of SCB, (**b**) SEM image of PB-SCB, (**c**) XRD pattern, and (**d**) FT-IR spectrum

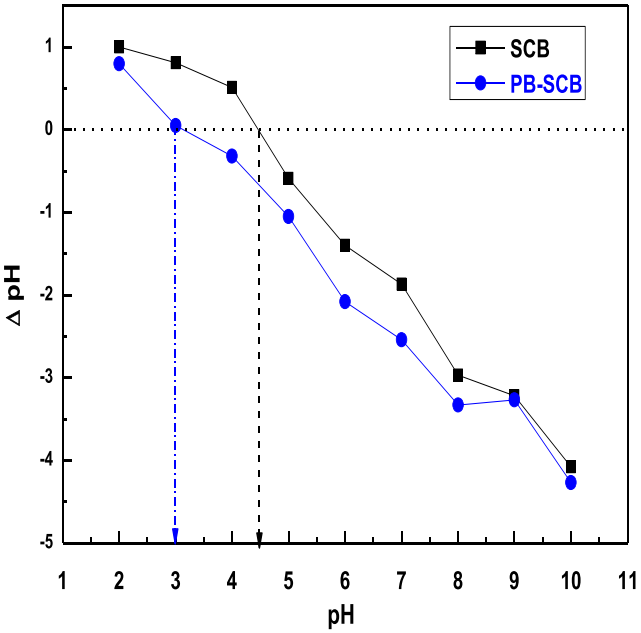

Fig. 4 Point of zero charge of SCB and PB-SCB adsorbents

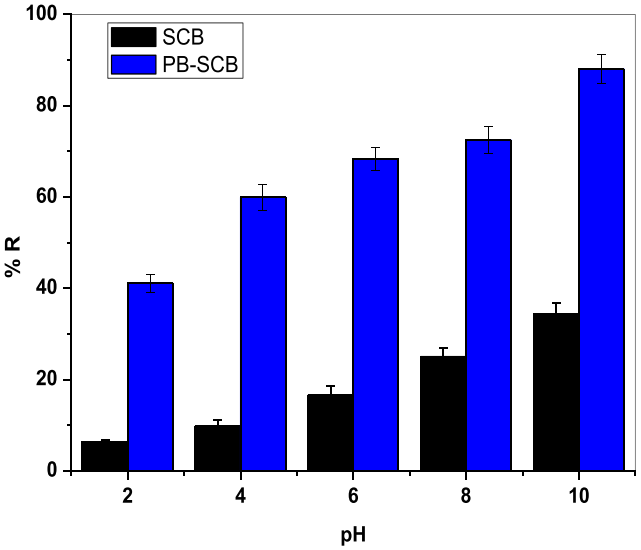

Fig. 5 Effect of solution pH on the adsorptive removal of cesium

enhanced (Metwally et al. 2019). On the other hand, at pH values below this point, the adsorption of positive charge substances will be negatively affected because the surface charge will be positive. As can be seen in Fig. 4, the pH_{Pzc} of SCB and PB-SCB are 4.5 and 3, respectively, indicating that PB-SCB will have better adsorption efficiency profiles than SCB at pH > 3.

Batch experiments

Batch technique tests were applied to evaluate the adsorption behaviors of inactive Cs(I) on the prepared PB-SCB adsorbent. In this respect, different effective parameters like solution pH, contact time, metal ion concentration, adsorbent dose, temperature, and the presence of interfering ions on the uptake process were optimized.

Influence of initial pH

The environmental pH has an overwhelming effect on the adsorption process, because the solubility of heavy metal ions, ionization of functional groups on the adsorbent surface, and charges of adsorption sites depend entirely on the solution pH (Ren et al. 2016). Therefore, it is vitally important to adjust the optimal pH value of the solution. As can be seen in Fig. 5, the adsorptive removal of Cs ions using both SCB and PB-SCB increased substantially as the solution pH values increased. In the case of using SCB, the removal efficiency for Cs ions was less than 10% at pH values below the SCB point of zero charge (pH_{Pzc} = 4.5) because the surface charge was positive below this point. However, when the solution pH was > pH_{Pzc}, the surface charge was negative; therefore, the removal efficiency of Cs ions gradually increased reaching to 30% at pH 10. In the case of using PB-SCB, at pH values below its pH_{Pzc}, the adsorptive removal efficiency of Cs ions was only around 40% as the electrostatic interaction between Cs ions and the PB-SCB was relatively hindered because the surface charge was positive; however, at pH values beyond 3, the removal efficiency of Cs ions increased significantly, reaching to around 90%, owing to the surface charge that was negatively charged. Overall, it can be observed that the capability of using PB-SCB to capture Cs ions from alkaline solutions was at least three times higher than that of applying SCB. Hence, these results confirmed that PB-SCB could be used in an alkaline solution to remove cesium ions.

Influence of contact time and adsorption kinetics

The adsorption capacity and removal efficiency of the prepared PB-SCB for Cs ions as a function of time were examined. Figure 6 a shows that the adsorption efficiency of the adsorbent increased rapidly over time, which attained after 2 h at 87.4% and reached equilibrium. It might be attributed to the existing of numerous vacant active sites on the surface of the adsorbent in the initial stage, which were occupied by the metal ions with the increase in the contact time (Karkehabadi et al. 2016). Therefore, in the next experiments, a contact time of 2 h was chosen for cesium adsorption.

The adsorption performance and kinetic mechanism of cesium ions on the prepared PB-SCB were investigated using pseudo-first-order (Lagergren 1898), pseudo-second-order (Yuh-Shan and Gordon 1999), and intraparticle diffusion (Weber and Morris 1963) models. The nonlinear forms of the former two models are given in Eqs. (6) and (7) respectively, and the latter model is shown in Eq. (8).

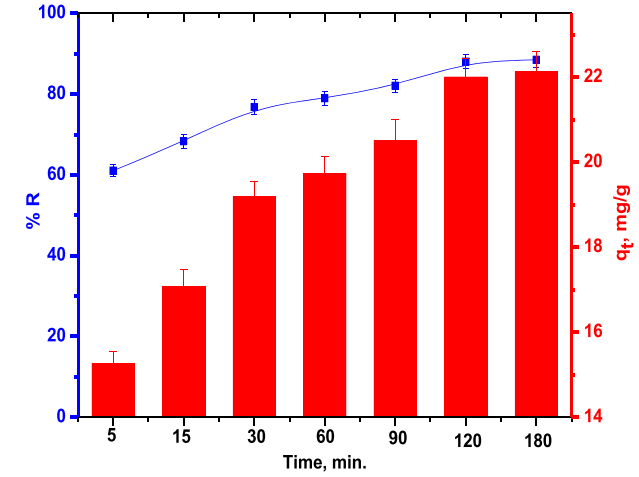

(a) Effect of contact time

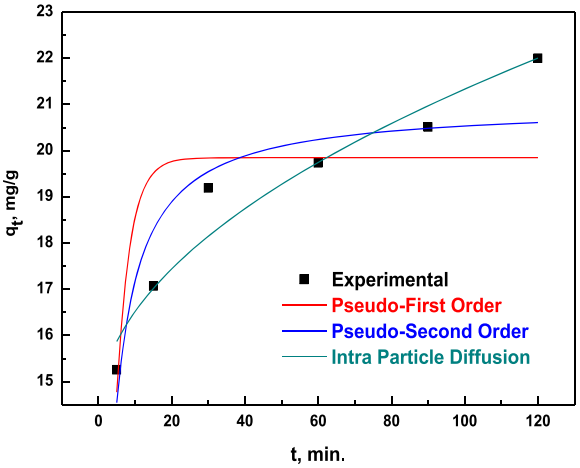

(b) Nonlinear kinetics models

Fig. 6 (**a**) Effect of contact time, and (**b**) Nonlinear kinetics models

Table 1 Kinetic parameters of the removal of Cs^+ from alkaline solutions

Kinetic models	Parameters	
Pseudo-first-order	q_e (mg/g)	22.20
	q_{cal} (mg/g)	19.85
	K_1 (1/min)	0.27
	R^2	0.51
Pseudo-second-order	q_e (mg/g)	22.20
	q_{cal} (mg/g)	20.99
	K_2 (mg/(g.min))	0.02
	R^2	0.82
Intra-particle diffusion	K_{ipd}	0.70
	R^2	0.93
	I (mg/g)	14.29

$$q_t = q_e\left(1-\exp^{-K_1 t}\right) \quad (6)$$

$$q_t = \left(K_2\, q_e{}^2\, t\right)/\left(1 + K_2\, q_e\, t\right) \quad (7)$$

$$q_t = K_{id}\, t^{0.5} + I \quad (8)$$

where q_t and q_e are the adsorption capacities (mg/g) at t (min) and at equilibrium, while I is the interparticle diffusion model intercept (mg/g), K_1 (1/min), K_2 (g/(mg.min)), and K_{id} (mg/(g.min)) are the investigated three models rate constants, respectively.

Table 1 and Fig. 6 outline the three investigated models' parameters. According to the obtained experimental data, the adsorption of cesium ions on PB-SCB was explained better and fitted to the pseudo-second-order model with higher correlation coefficient reached 0.82 compared to pseudo-first-order model which was 0.51 meaning chemical adsorption mechanism played a considerable role in the process which is consistent with other reports (Jang and Lee 2016) to remove cesium ions. Moreover, the experimental and calculated capacity values in the case of pseudo-second-order are more close to each other compared with that of pseudo-first-order model. The straight line obtained in the case of intraparticle diffusion model linear fitting implied that intraparticle diffusion participated in the adsorption mechanism, but it is not the only rate controlling step because this line did not pass through the origin.

Influence of PB-SCB adsorbent dosage

An important factor that affects the adsorption capacity and the removal % of Cs^+ using PB-SCB is the adsorbent dose. In Fig. 7, by increasing PB-SCB dose, the adsorption capacity decreased from 28.69 to 11.60 mg/g, while the adsorption % increased from 57.38 to 92.86%. This is because of a portion

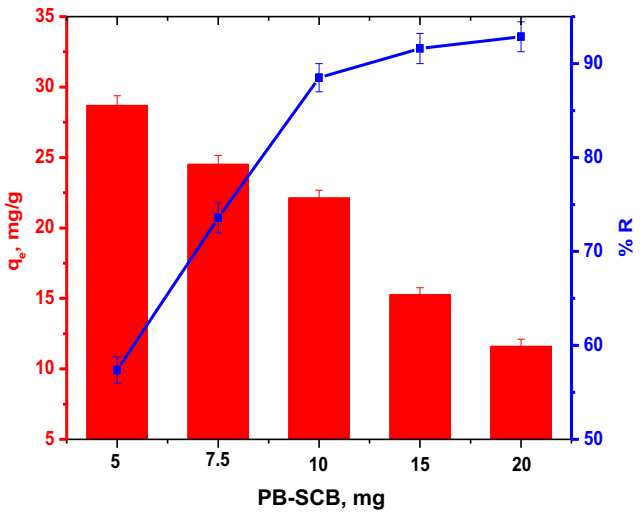

Fig. 7 Effect of adsorbent dose on the adsorption of Cs(I)

of the adsorption remained unsaturated when the adsorbent dose increased, and this outcome in better removal percentage. Keeping the concentration of Cs^+ constant, the increase in PB-SCB dose may cause particulate accumulation of its adsorption sites resulting in a decrease in the total adsorbent surface area available for Cs^+ ion removal (Kumar et al. 2009). From the economic perspective, 10 mg was considered through other experiments.

Influence of Cs(I) ion concentration and isotherm study

The investigation of Cs^+ initial concentration effect on the adsorption process was studied. As shown in Fig. 8a, Cs^+ adsorption capacity increased with increasing initial concentration and reached 56.7 mg/g. This well-known phenomenon may be attributed to the existing of a large number of accessible Cs^+ ions near the adsorbent leading to a high driving force for mass transfer before the adsorption-desorption equilibrium (Karkeh-abadi et al. 2016). Moreover, the adsorption efficiency decreased as the initial concentration of the Cs^+ ions increased, indicating that the available adsorption sites became occupied (Ararem et al. 2011).

Equilibrium studies for the adsorption of Cs(I) were examined to clarify the adsorption mechanism using three different isotherm models, Langmuir (1918), Freundlich (1906), and Dubinin-Radushkevich (D-R) (Dubinin and Radushkevich 1947), where the mathematical nonlinear forms of these models are represented in Eqs. (9), (10), and (11), respectively. Although Langmuir model assumes a monolayer formed by adsorbate around the homogenous surface of the adsorbent

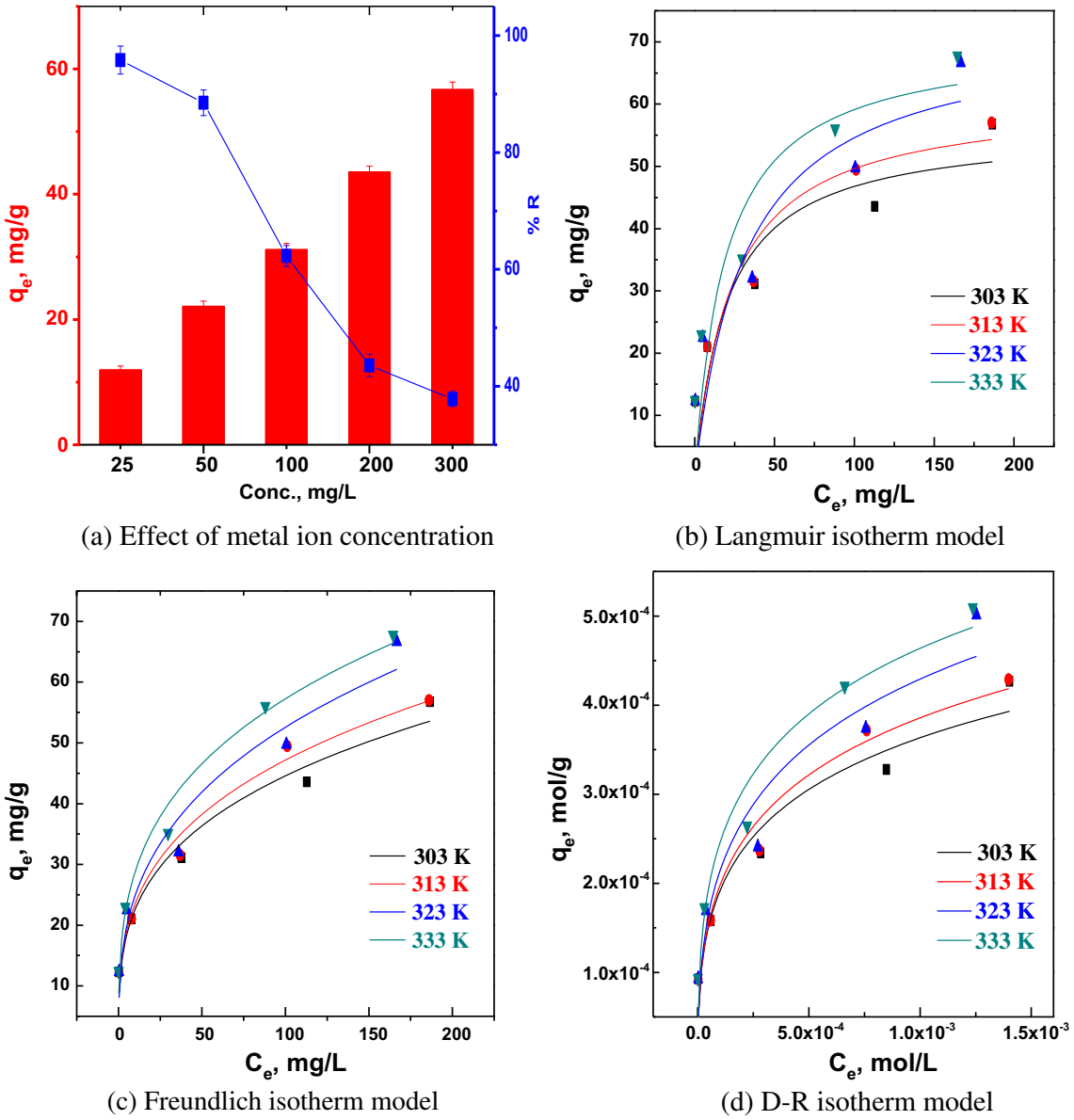

Fig. 8 (**a**) Effect of metal ion concentration, (**b**) Langmuir, (**c**) Freundlich, and (**d**) D-R isotherm models

without interaction between them, Freundlich model supposes a heterogeneous surface multilayer adsorption process, based on strong electrostatic interaction between positive and negative charges (Liu and Zhang 2015). In the D-R adsorption isotherm, E_a can be utilized to decide the adsorption mechanism to be physical or chemical (Ren et al. 2016). When $1 < E_a < 8$, the dominant adsorption process mechanism will be physical; however, in the case of $8 < E_a < 16$, the dominant mechanism will be an ion exchange (chemical) (Alipour et al. 2016).

$$q_e = (C_e b q_m)/(1 + C_e b) \quad (9)$$

$$q_e = K_F C_e^{1/n} \quad (10)$$

$$q_e = q_m \exp\left(-\delta \left(\mathrm{RT} \ln(1 + (1/C_e))^2\right)\right) \quad (11)$$

where C_e represents the equilibrium concentration in (mg/L) for Eqs. (9) and (10) and in (mole/L) for Eq. (11). q_e (adsorption capacity at equilibrium) and q_m (maximum adsorption capacity) are given in (mg/g) for Eqs. (9) and (10) and in (mole/g) for Eq. (11), where b is the Langmuir equilibrium constant, n and K_F are the Freundlich isotherm constants. R is the rate gas constant (8.314 kJ/(mol.K)), and T is the temperature in kelvin (K). δ value can be utilized to calculate the mean energy of adsorption ($E_a = (1/(2\ \delta)^{0.5})$ (kJ/mol).

The adsorption plots and the fitting model parameters with R^2 for the diverse models were independently shown in Fig. 8 and Table 2. In terms of R^2 values, the applicability of the above 3 models for present experimental data approximately followed the order: Freundlich > D-R > Langmuir. Based on these obtained data, the adsorption mechanism of Cs^+ seems to follow the Freundlich isotherm with higher correlation coefficients R^2 (0.98) rather than that of Langmuir isotherm R^2 (0.81) suggesting multilayer adsorption being more predominant with an agreement with other studies using PB-based adsorbents to remove cesium ions (Cho et al. 2018). The values of n in the Freundlich equation over the range of 1 to 10 explain that the adsorption is favorable. As shown in Table 2, the n values at all 4 temperatures were in this range illustrating that PB-SCB adsorbent had good adsorption characteristics toward Cs^+. According to the analysis of the D-R model, the E_a value was ranged from (13–14) kJ/mol which indicated that the adsorption behavior of cesium on PB-SCB could be described as chemical adsorption, which is in good agreement with kinetic models. These results well agreed with the observations of previous reports for the adsorption of cesium onto other adsorbents (Wang et al. 2019). The maximum adsorption capacity calculated by the Langmuir at 303 K is 56.21 mg/g, which is very close to the value actually determined as 56.7 mg/g.

Table 2 Langmuir, Freundlich, and D-R isotherm parameters

Isotherm model	Parameters	Temperature			
		303	313	323	333
Langmuir	q_m (mg/g)	56.21	60.99	72.12	70.55
	R^2	0.75	0.81	0.72	0.79
Freundlich	K_f (L/g)	11.45	11.70	11.69	14.51
	n	3.39	3.30	3.06	3.35
	R^2	0.96	0.97	0.94	0.98
D-R	q_m (mg/g)	110.39	121.45	140.98	139.65
	δ (mol^2/KJ^2)	2.73E-9	2.67E-9	2.62E-9	2.54E-9
	E_a (kJ/mol)	13.53	13.68	13.81	14.03
	R^2	0.92	0.94	0.89	0.94

Influence of temperature and thermodynamic study

The influence of temperature was optimized for Cs^+ adsorption on PB-SCB adsorbent. Figure 9 a illustrates that, with the rise of temperature, the adsorption capacity of PB-SCB adsorbent and Cs(I) removal rate increased slightly, reaching 38 mg/g and 94%, respectively. This is may be because the increase of the adsorbent active sites at elevated temperature enhanced the adsorption capacity of Cs(I) ions (Chen et al. 2010).

The impact of temperature on the adsorption reaction can be assessed using the adsorption thermodynamic parameters. Therefore, Gibbs free energy change (ΔG), standard enthalpy (ΔH), and standard entropy (ΔS) as thermodynamic parameters were calculated under different temperatures using the following equations:

$$\Delta G = -\mathrm{RT\ Ln}\ K_c \quad (12)$$

$$\Delta G = \Delta H - T\Delta S \quad (13)$$

where K_c is the equilibrium constant ($K_c = C_a/C_e$) (Kurniawan et al. 2011), C_a and C_e are the concentration of Cs^+ phase adsorbed on PB-SCB at equilibrium (mg/L), and the equilibrium concentration of Cs^+ in solution (mg/L), respectively, R represents the universal gas constant (8.314 J/(mol.K)), and T is the absolute temperature in Kelvin (K). Figure 9 b explains the plot of ΔG versus T in which the values of ΔH and ΔS can be determined from the slope and intercept that were tabulated in Table 3. While the negative values of ΔG confirmed that the adsorption of cesium ions using PB-SCB is spontaneous in nature, the positive value of ΔH indicated that the adsorption process is endothermic.

It was previously reported that physical adsorption occurred when $(\Delta G) \leq -20$ (KJ/mol), while at $(\Delta G) \geq -40$ (KJ/mol) (chemical adsorption) is dominated the adsorption process. The (ΔG) values obtained in this study are < -10 (KJ/mol), indicative that physical adsorption is included in the sorption process.

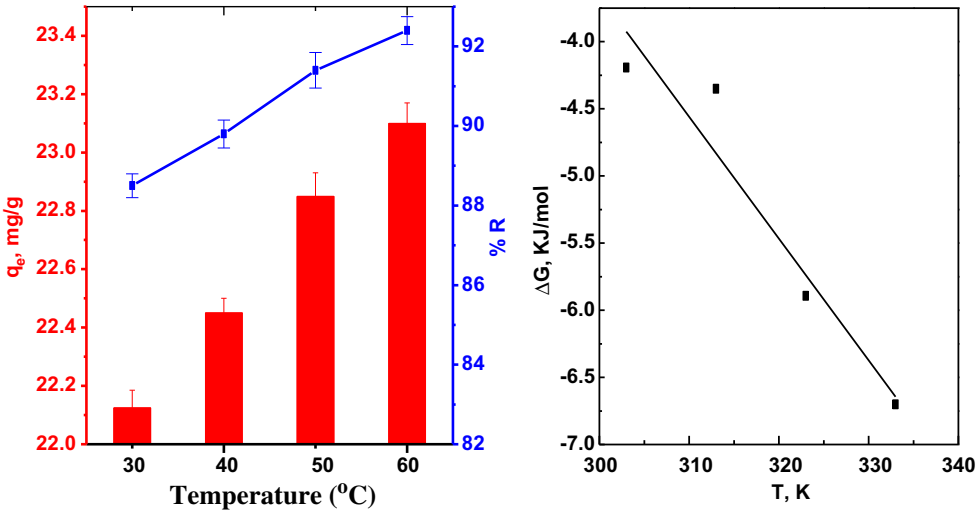

(a) Effect of temperature (b) Thermodynamic

Fig. 9 (**a**) Effect of temperature, and (**b**) thermodynamic parameters on adsorption of Cs(I) ions

Effect of interfering cations

The electrostatic interaction, ionic strength, and hydrated radius are significant factors, as physisorption (ion trapping) and chemisorption (ion exchange) are important for cesium adsorption. The distribution coefficient of Cs^+ on the optimal mixture as a function of Li^+, Na^+, and K^+ concentration is shown in Fig. 10a. The obtained results clarified that there was no significant change (only less than 2%) in the K_d values of Cs^+ at the investigated range concentration in the case of Li^+ and Na^+ solution. However, the more decrease in the K_d values of Cs^+ can be obviously observed in the case of using K^+ ions, where there was around 10% decrease when the concentration of K^+ increased to 100 mg/L. This can be clarified by the way that the higher charge density ions (Fig. 10b) can bind to larger water clusters; hence, the change in the K_d values could follow the order of hydrated ionic radii sequence $Li^+ > Na^+ > K^+ > Cs^+$ (Jr 1959). Thus, the competitive adsorption capacity of the present ions decreased in the order $K^+ > Na^+ > Li^+$, which is consistent with the experimental results and other previous reports (Wang et al. 2019). However, the concentration of K^+ in radioactive wastes is much lower than that of other cations; hence, the prevention of cesium adsorption by K^+ will not be a significant issue in real applications (Attallah et al. 2011).

Table 3 Thermodynamic parameters for the adsorption of Cs(I)

T (K)	ΔG (kJ/mol)	ΔH (kJ/mol)	ΔS (KJ/(mol.K))	E_a (KJ/mol)
303	− 4.19	21.2	0.08	5.06 E-05
313	− 4.35			
323	− 5.89			
333	− 6.7			

The maximum adsorption of Cs(I) with various adsorbents

For comparison, the cesium adsorption capacities of previously reported adsorbents are given in Table 4. The maximum adsorption capacity of PB-SCB adsorbent was not the best among those reported in previous studies. However, the maximum adsorption capacity is not the only performance indicator, and we focused more on the simplicity, environmentally friendless, and the cost-effectiveness of the prepared adsorbent.

Mechanism

The binding mechanism of Cs^+ ions on PB remains controversial. Some researchers suppose that Cs^+ ions are adsorbed into the crystal cage structure of metal hexacyanoferrate as an ion pair with a cation (physical adsorption) (Ishizaki et al. 2013), whereas others consider that Cs^+ ions are exchanged with K^+ ions (chemical adsorption) (Avramenko et al. 2011), particularly on the adsorbent surface layer. FT-IR and EDS investigation (Fig. 11a, b, respectively) were performed to propose the adsorption mechanism of Cs^+ ions onto PB-SCB. FT-IR spectra of Cs-laden samples showed no obvious changes in the vibration bands indicating the non-participation of the functional groups located on the surface of PB-SCB for the removal of Cs^+ ions (Zong et al. 2017). Moreover, EDS spectra explained elevated peaks of Cs on PB-SCB (Fig. 11b), which were not clear on the PB-SCB before adsorption. These elevated peaks of Cs^+ have associated with the lowering of other peaks, e.g., K^+ peaks present in pre-sorption samples. This result approved the involvement of the ion exchange mechanism between K^+ and Cs^+ during sorption onto PB-SCB, in which the element content of K^+ and Cs^+ before and after the reaction was

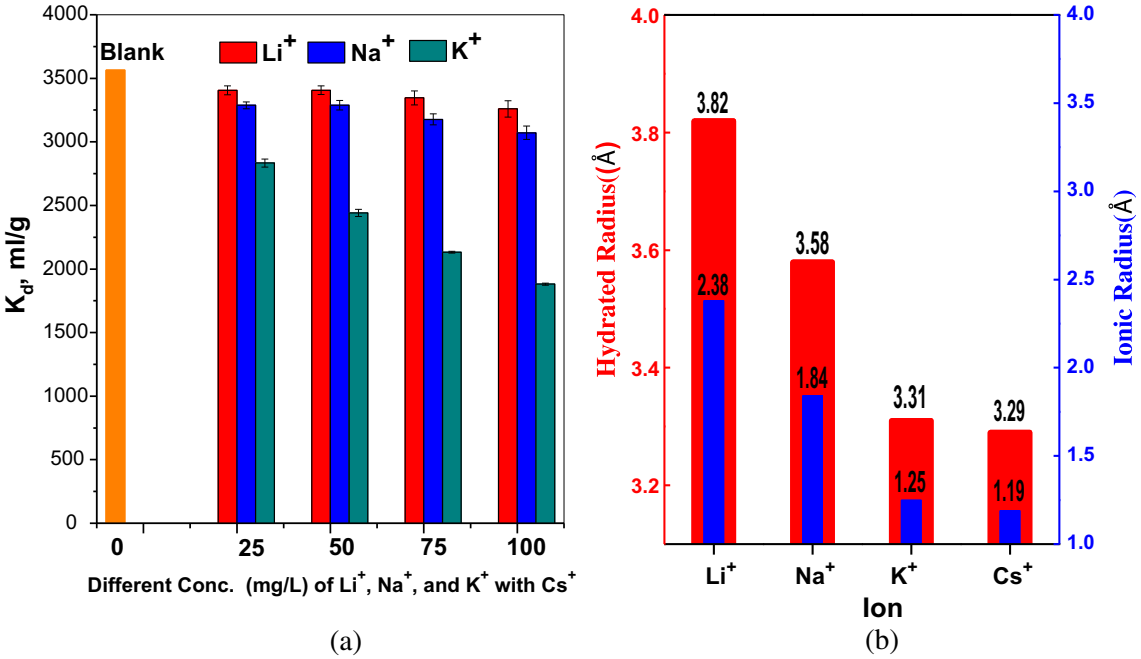

Fig. 10 Effect of interfering cations on the adsorption of Cs(I): (**a**) Different Conc. (mg/L), and (**b**) Ionic radius

changed from 1.90 to 0.66% for K^+ and from 0 to 8.82% for Cs^+. On the other hand, the conjunction of the adsorption kinetic (pseudo-second-order), isotherms (Dubinin and Radushkevich), and thermodynamics with the analysis of EDS in this study elucidated that the removal mechanism of Cs^+ by PB-SCB might be the joint action of chemisorption (K-exchange) and physisorption (ion-trapping), which is in good agreement with other reports (Alamudy and Cho 2018). Therefore, Cs^+ ions would be efficiently adsorbed at the crystal lattice spaces by the proton-exchange mechanism, not the electrostatic attraction (Jang et al. 2015) as clearly illustrated in Fig. 12.

Radioactive ^{137}Cs removal

The PB-SCB adsorbent was applied for the removal of a real radioactive ^{137}Cs sample. In this respect, different samples with activity 140×10^3 Bq/L of radioactive ^{137}Cs were mixed with different weights of PB-SCB adsorbent (0.01, 0.05 g) and shaked for different times. After the separation of the

Table 4 Maximum adsorption capacity of cesium in various adsorbents

Adsorbent	Adsorption parameters			Adsorption capacity (mg/g)	Ref.
	Cs ion concentration	pH	Adsorbent dose		
PB-SCB adsorbent	300 mg/L	10	2 g/L	56.7	Present study
Photocatalytic-PB/TiO_2	6.65 mg/L	NR	5 g/L	1.2	(Kim et al. 2018)
PB/GO foam	500 mg/L	NR	2 g/L	18.67	(Jang et al. 2015)
Ammonium-pillared MMT/Fe_3O_4 composite	40 mg/L	6.7	0.5 g/L	27.53	(Zheng et al. 2017)
CMC/PB-La	140 mg/L	7	1 g/L	35.22	(Zong et al. 2017)
PB/Fe_3O_4/GO/alginate	150 mg/L	7	2.5 g/L	43.52	(Yang et al. 2014)
Ammonium molybdophosphate–polyacrylonitrile	200 mg/L	7.5	2 g/L	78.17	(Long et al. 2014)
Ethylamine-modified MMT	340 mg/L	7.5	2 g/L	80.27	(Long et al. 2013)
PB-coated magnetic nanoparticles	2780 mg/L	NR	6.25 g/L	96	(Thammawong et al. 2013)

NR not reported

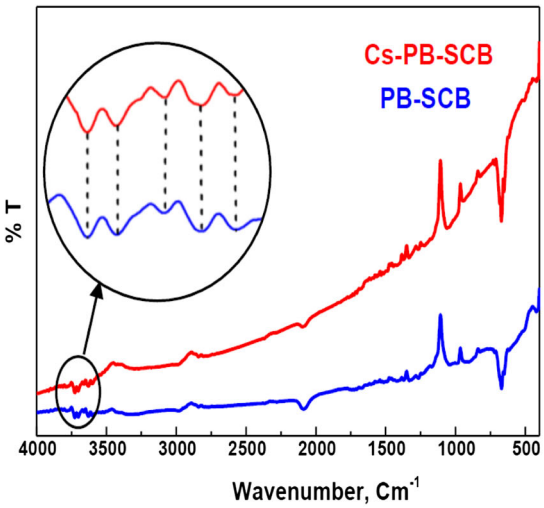

(a) FT-IR spectra of PB-SCB before and after Cs (I) adsorption

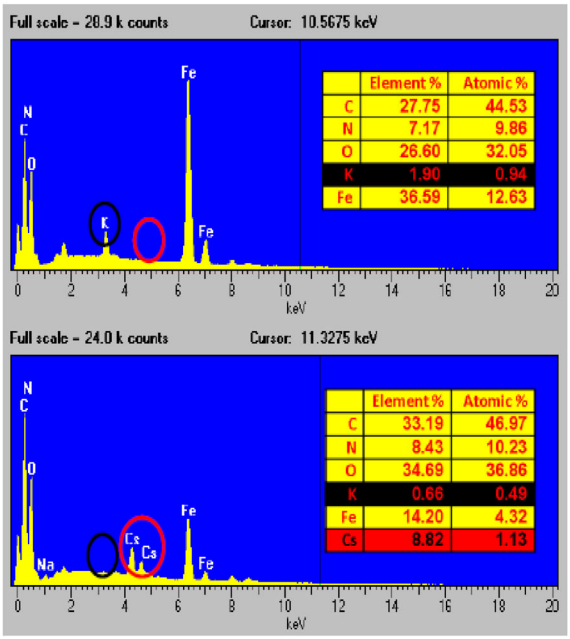

(b) EDS analysisof PB-SCB before and after Cs (I) adsorption

Fig. 11 (**a**) FT-IR spectra, and (**b**) EDS analysis before and after Cs ions adsorption on the PB-SCB backbone

adsorbent from the liquid phase, the activity of the samples was measured by multichannel NaI (Tl) detector. The obtained results are illustrated in Fig. 13.

It was found that the activity of the solution dropped by more than 95% (from 280 down to 11.2 Bq) using 0.05 mg of the composite (Fig. 13b), which was attributed to a large number of accessible adsorption sites. In addition, the high DF (25) further confirmed the promising application of the PB-SCB composite for the decontamination of ^{137}Cs containing radioactive wastewater which is 13.88-fold higher than that of in case using cellulose/HO_7Sb_3 nanocomposite (Abdel-Galil et al. 2018) and 10 times as high as that of in case using aluminum silicate modified by magnesia (Mansy et al. 2017) for the removal of ^{137}Cs from radioactive wastewater. Moreover, in the case of the dynamic removal of 50 ml ^{137}Cs (with total activity of 7000 Bq), the applicability of the PB-SCB to decontaminate radiocesium ions from real radioactive wastewater was confirmed by the outstanding drop in the total 50-ml activity (from 7000 to almost 250 Bq), a decline of more than 96% in just 20 min, resulting in a high DF (27.8) (Fig. 13a).

Cost analysis and applicability

The price of any adsorbent plays an important role when it is to be used for detoxification of contaminants from wastewater in large-scale implementation. Hence, there are several factors

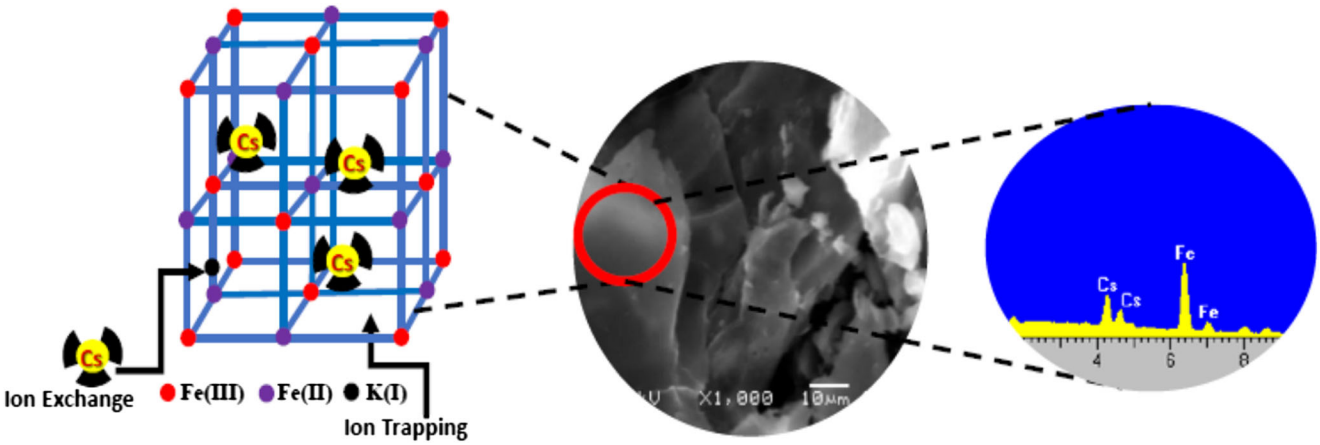

Fig. 12 Proposed mechanism of the PB-SCB to remove cesium ions

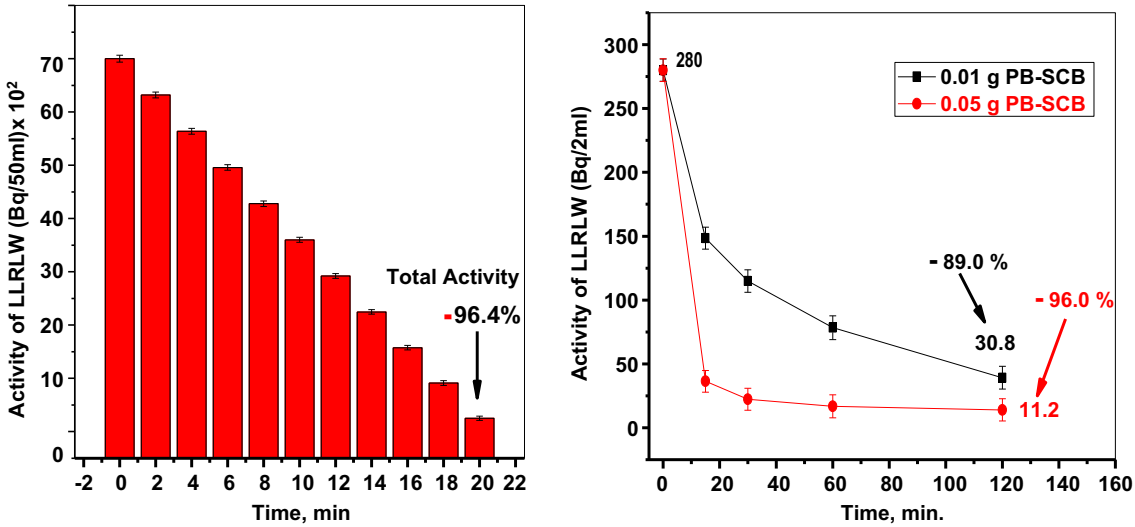

(a) Dynamic studies (b) Application static

Fig. 13 Removal of ^{137}Cs from real radioactive liquid waste sample: (**a**) Dynamic studies, and (**b**) Application static

that governed the cost of any adsorbent material, like energy consumed and the precursors used. SCB is readily available in abundance as waste at no cost; therefore, the main cost will come from the using of the reagents to be used in the synthesis of PB. The overall cost can be calculated using Eq. (14) (Dalvand et al. 2011).

$$\text{Operating Cost} = \sum C_{\text{reagents}} + C_{\text{Energy}} \quad (14)$$

where C_{energy} denotes the cost of energy consumed and C_{reagents} represents the sum of the cost of the used reagents. The rate of electricity US$0.13/kW was used in the calculations as used by Saad et al. (2017).

As the maximum adsorption capacity of PB-SCB for the removal of Cs is 56.7 mg/g at 30 °C, therefore, an approximate amount of PB-SCB (17.5 g) will be required to decontaminate 1000 mg of Cs. The approximate consumption and evaluated cost for the treatment of Cs-decontaminated wastewater (1000 mg) at the optimum operating parameters is presented in Table 5, where the prices were obtained from Alibaba website as an actual estimation for the market price as previously approved by several authors (Thompson et al. 2016; Borra et al. 2016).

Considering the benefits of PB-SCB preparation and eco-friendless, the analysis revealed that the proposed method is not only efficient for the significant removal of radio-cesium but also it is among the least expensive methods available for the said purpose. The total cost was determined to be only US$0.12 for the treatment of 1000 mg cesium-containing alkaline solution, confirming that our proposed material is considered to be among the cheapest adsorbents available for wastewater treatment.

Table 5 Approximate cost estimation for the all used reagents

	Price (US$)/unit	Amount consumed	Cost (US$)
Process/precursor			
SCB collection	Bio-waste	Free	0.000
Washing and drying	Tap Water and Sun	Free	0.000
Boiling	0.13/kW	0.25 kW	0.033
$K_4[Fe(CN)_6]\cdot 3H_2O$	2.25/kg	2.84×10^{-3} kg	0.006
$Fe(NO_3)_3\cdot 9H_2O$	0.56/kg	3.59×10^{-3} kg	0.002
Stirring over night	0.13/kW	0.54 kW	0.070
Net cost			0.111
Overhead cost (10% of net cost)			0.011
Final cost			0.122

Conclusion

Prussian blue nanoparticles functionalized sugarcane bagasse was successfully prepared for the removal of radioactive cesium (^{137}Cs). According to the obtained results, PB-SCB adsorbent showed enhanced adsorption toward cesium in the presence of competing cations with adsorption capacity reached to 56.7 mg/g. Therefore, the PB-SCB adsorbent could be widely applied in large-scale applications for the decontamination of radioactive cesium from alkaline solutions because of the simple and environmentally friendly synthetic method, and the costless of sugarcane bagasse.

Acknowledgments Authors are thankful to the Department of Analytical Chemistry and Control, Hot Laboratories and Waste Management Center

for kind cooperation and help in providing necessary laboratory facilities to carry out this work.

Funding This research did not receive any specific grant from funding agencies in the public, commercial, or not-for-profit sectors.

Compliance with ethical standards

Conflict of interest The authors declare that they have no conflict of interest.

References

Abdel-Galil EA, Moloukhia H, Abdel-Khalik M, Mahrous SS (2018) Synthesis and physico-chemical characterization of cellulose/HO_7Sb_3 nanocomposite as adsorbent for the removal of some radionuclides from aqueous solutions. Appl Radiat Isotopes 140:363–373

Alamudy HA, Cho K (2018) Selective adsorption of cesium from an aqueous solution by a montmorillonite-prussian blue hybrid. Chem Eng J 349:595–602

Alipour D, Keshtkar AR, Moosavian MA (2016) Adsorption of thorium (IV) from simulated radioactive solutions using a novel electrospun PVA/TiO2/ZnO nanofiber adsorbent functionalized with mercapto groups: study in single and multi-component systems. Appl Surf Sci 366:19–29

Ararem A, Bouras O, Arbaoui F (2011) Adsorption of caesium from aqueous solution on binary mixture of iron pillared layered montmorillonite and goethite. Chem Eng J 172(1):230–236

Attallah MF, Borai EH, Allan KF (2009) Kinetic and thermodynamic studies for cesium removal from low-level liquid radioactive waste using impregnated polymeric material. Radiochemistry 51:622–627

Attallah MF, Borai EH, Hilal MA, Shehata FA, Abo-Aly MM (2011) Utilization of different crown ethers impregnated polymeric resin for treatment of low level liquid radioactive waste by column chromatography. J Hazard Mater 195:73–81

Avramenko V, Bratskaya S, Zheleznov V, Sheveleva I, Voitenko O, Sergienko V (2011) Colloid stable sorbents for cesium removal: preparation and application of latex particles functionalized with transition metals ferrocyanides. J Hazard Mater 186(2–3):1343–1350

Basu H, Saha S, Pimple MV, Singhal RK (2018) Graphene-Prussian blue nanocomposite impregnated in alginate for efficient removal of cesium from aquatic environment. J Environ Chem Eng 6(4):4399–4407

Borai EH, Hilal MA, Attallah MF, Shehata FA (2008) Improvement of radioactive liquid waste treatment efficiency by sequential cationic and anionic ion exchangers. Radiochim Acta 96:441–447

Borra CR, Mermans J, Blanpain B, Pontikes Y, Binnemans K, Gerven TV (2016) Selective recovery of rare earths from bauxite residue by combination of sulfation, roasting and leaching. Miner Eng 92:151–159

Calarese E (2011) Improving the scientific foundations for estimating health risks from the Fukushima incident. Proc Natl Acad Sci U S A 108(49):19447–19448

Chang S, Chang L, Han W, Li Z, Dai Y, Zhang H (2018) In situ green production of Prussian blue/natural porous framework nanocomposites for radioactive Cs^+ removal. J Radioanal Nucl Chem 316(1):209–219

Chen JH, Li GP, Liu QL, Ni JC, Wu WB, Lin JM (2010) Cr(III) ionic imprinted polyvinyl alcohol/sodium alginate (PVA/SA) porous composite membranes for selective adsorption of Cr(III) ions. Chem Eng J 165:465–473

Cho E, Kim J, Park CW, Lee K, Lee TS (2018) Chemically bound Prussian blue in sodium alginate hydrogel for enhanced removal of Cs ions. J Hazard Mater 360:243–249

Dalvand A, Gholami M, Joneidi A, Mahmoodi NM (2011) Dye removal, energy consumption and operating cost of electrocoagulation of textile wastewater as a clean process. Clean-Soil Air Water 39(7):665–672

Ding N, Kanatzidis MG (2010) Selective incarceration of caesium ions by Venus flytrap action of a flexible framework sulfide. Nat Chem 2:187–191

Dubinin MM, Radushkevich LV (1947) Equation of the characteristic curve of activated charcoal. Proc Acad Sci USSR 55:331–333

Freundlich HMF (1906) Over the adsorption in solution. J Phys Chem 57(385471):1100–1107

Igberase E, Osifo P (2015) Equilibrium, kinetic, thermodynamic and desorption studies of cadmium and lead by polyaniline grafted cross-linked chitosan beads from aqueous solution. J Ind Eng Chem 26:340–347

Ishizaki M, Akiba S, Ohtani A, Hoshi Y, Ono K, Matsuba M, Togashi T, Kananizuka K, Sakamoto M, Takahashi A, Kawamoto T, Tanaka H, Watanabe M, Arisaka M, Nankawa T, Kurihara M (2013) Proton-exchange mechanism of specific Cs^+ adsorption via lattice defect sites of Prussian blue filled with coordination and crystallization water molecules. Dalton T 42(45):16049–16055

Jang J, Lee DS (2016) Magnetic Prussian blue nanocomposites for effective cesium removal from aqueous solution. Ind Eng Chem Res 55(13):3852–3860

Jang SC, Haldorai Y, Lee GW, Hwang SK, Han YK, Roh C, Huh YS (2015) Porous three-dimensional graphene foam/prussian blue composite for efficient removal of radioactive ^{137}Cs. Sci Rep 5:17510

Jr ERN (1959) Phenomenological theory of ion solvation. Effective radii of hydrated ions. J Phys Chem 63(9):1381–1387

Karkeh-abadi F, Saber-Samandari S, Saber-Samandari S (2016) The impact of functionalized CNT in the network of sodium alginate-based nanocomposite beads on the removal of Co(II) ions from aqueous solutions. J Hazard Mater 312:224–233

Kawamoto T, Tanaka H, Watanabe H, Sugiyama Y, Hattori T, Matsuzaki S, Shibaba M (2012) Granular adsorbent for r-Cs with inorganic binder. Patent:JPA2012–J250904

Kim H, Kim M, Kim W, Lee W, Kim S (2018) Photocatalytic enhancement of cesium removal by Prussian blue-deposited TiO_2. J Hazard Mater 357:449–456

Kumar M, Tripathi BP, Shahi VK (2009) Crosslinked chitosan/polyvinyl alcohol blend beads for removal and recovery of Cd (II) from wastewater. J Hazard Mater 172(2–3):1041–1048

Kurniawan A, Kosasih AN, Febrianto J, Ju YH, Sunarso J, Indraswati N, Ismadji S (2011) Evaluation of cassava peel waste as lowcost biosorbent for Ni-sorption: equilibrium, kinetics, thermodynamics and mechanism. Chem Eng J 172:158–166

Lagergren S (1898) Zur theorie der sogenannten adsorption geloster stoffe. Kungliga Svenska Vetenskapsakademiens Handlingar 24:1–39

Langmuir I (1918) The adsorption of gases on plane surfaces of glass, mica and platinum. J Am Chem Soc 40(9):1361–1403

Li G, Wang M, Chen X, Li X (2017) Adsorption performance for the removal of Cu (II) on the ammonium acetate modified sugarcane bagasse. Nat Env & Poll Tech 16(3):843–848

Liu X, Zhang L (2015) Removal of phosphate anions using the modified chitosan beads: adsorption kinetic, isotherm and mechanism studies. Powder Technol 277:112–119

Long H, Wu P, Zhu N (2013) Evaluation of Cs^+ removal from aqueous solution by adsorption on ethylamine-modified montmorillonite. Chem Eng J 225:237–244

Long H, Wu P, Yang L, Huang Z, Zhu N, Hu Z (2014) Efficient removal of cesium from aqueous solution with vermiculite of enhanced

adsorption property through surface modification by ethylamine. J Colloid Interface Sci 428:295–301

Manolopoulou M, Vagena E, Stoulos S, Ioannidou A, Papastefanou C (2011) Radioiodine and radiocesium in Thessaloniki, northern Greece due to the Fukushima nuclear accident. J Environ Radioact 102:796–797

Mansy MS, Hassan RS, Selim YT, Kenawy SH (2017) Evaluation of synthetic aluminum silicate modified by magnesia for the removal of ^{137}Cs, ^{60}Co and $^{152+154}Eu$ from low-level radioactive waste. Appl Radiat Isotopes 130:198–205

Metwally SS, El-Sherief EA, Mekhamer HS (2019) Fixed-bed column for the removal of cesium, strontium, and lead ions from aqueous solutions using brick kiln waste. Sep Sci Technol:1–13

Mihara Y, Sikder Md T, Yamagishi H, Sasaki T, Kurasaki M, Itoh S, Tanaka S (2016) Adsorption kinetic model of alginate gel beads synthesized micro particle-Prussian blue to remove cesium from water. J Water Process Eng 10:9–19

Ming-hua T, Yi-fen G, Cheng-yao S, Chang-qing Y, De-chang W (1988) Measurement of internal contamination with radioactive caesium released from the Chernobyl accident and enhanced elimination by Prussian blue. J Radiol Prot 8(1):25–28

Neroda AS, Mishukov VF, Goryachev VA, Simonenkov DV, Goncharova AA (2014) Radioactive isotopes in atmospheric aerosols over Russia and the sea of Japan following nuclear accident at Fukushima Nr. 1 Daiichi Nuclear Power Station in March 2001. Environ Sci Pollut Res 21:5669–5677

Noor NM, Othman R, Mubarak NM, Abdullah EC (2017) Agricultural biomass-derived magnetic adsorbents: preparation and application for heavy metals removal. J Taiwan Inst Chem E 78:168–177

Oliveira AR, Hunt JG, Valverde NJ, Brandao-Mello CE, Farina R (1991) Medical and related aspects of the Goiania accident: an overview. Health Phys 60(1):17–24

Parajuli D, Takahashi A, Noguchi H, Kitajima A, Tanaka H, Takasaki M, Yoshino K, Kawamoto T (2016) Comparative study of the factors associated with the application of metal hexacyanoferrates for environmental Cs decontamination. Chem Eng J 283:1322–1328

Ren H, Gao Z, Wu D, Jiang J, Sun Y, Luo C (2016) Efficient Pb(II) removal using sodium alginate-carboxymethyl cellulose gel beads: preparation, characterization, and adsorption mechanism. Carbohyd Polym 137:402–409

Saad M, Tahir H, Ali D (2017) Green synthesis of Ag-Cr-Ac nanocomposites by Azadirachta indica and its application for the simultaneous removal of binary mixture of dyes by ultrasonicated assisted adsorption process using response surface methodology. Ultrason Sonochem 38:197–213

Sangvanich T, Sukwarotwat V, Wiacek RJ, Grudzien RM, Fryxell GE, Addleman RS, Timchalk C, Yantasee W (2010) Selective capture of cesium and thallium from natural waters and simulated wastes with copper ferrocyanide functionalized mesoporous silica. J Hazard Mater 182:225–231

Su S, Liu Q, Liu J, Zhang H, Li R, Jing X, Wang J (2018) Functionalized sugarcane bagasse for U(VI) adsorption from acid and alkaline conditions. Sci Rep 8(1):793–802

Thammawong C, Opaprakasit P, Tangboriboonrat P, Sreearunothai P (2013) Prussian blue-coated magnetic nanoparticles for removal of cesium from contaminated environment. J Nanopart Res 15:1689–1698

Thompson KA, Shimabuku KK, Kearns JP, Knappe DRU, Summers RS, Cook SM (2016) Environmental comparison of biochar and activated carbon for tertiary wastewater treatment. Environ Sci Technol 50(20):11253–11262

Vincent T, Taulemesse JM, Dauvergne A, Chanut T, Testa F, Guibal E (2014) Thallium(I) sorption using Prussian blue immobilized in alginate capsules. Carbohydr Polym 99:517–526

Vincent C, Barre Y, Vincent T, Taulemesse JM, Robitzer M, Guibal E (2015) Chitin-Prussian blue sponges for Cs(I) recovery: from synthesis to application in the treatment of accidental dumping of metal-bearing solution. J Hazard Mater 287:171–179

Vipin AK, Hu B, Fugetsu B (2013) Prussian blue caged in alginate/calcium beads as adsorbents for removal of cesium ions from contaminated water. J Hazard Mater 258:93–101

Wang K, Ma H, Pu S, Yan C, Wang M, Yu J, Wang X, Chu W, Zinchenko A (2019) Hybrid porous magnetic bentonite-chitosan beads for selective removal of radioactive cesium in water. J Hazard Mater 362:160–169

Weber WJ, Morris JC (1963) Kinetics of adsorption on carbon from solution. J Sanit Eng Div 89(2):31–60

Yang H, Li H, Zhai J, Sun L, Zhao Y, Yu H (2014) Magnetic Prussian blue/graphene oxide nanocomposites caged in calcium alginate microbeads for elimination of cesium ions from water and soil. Chem Eng J 246:10–19

Yang H, Li H, Zhai J, Yu H (2015) In situ growth of Prussian blue nanocrystal within Fe^{3+} crosslinking PAA resin for radiocesium highly efficient and rapid separation from water. Chem Eng J 277:40–47

Yu H, Hu J, Liu Z, Ju X, Xie R, Wang W, Chu L (2017a) Ion-recognizable hydrogels for efficient removal of cesium ions from aqueous environment. J Hazard Mater 323:632–640

Yu J, Xiong W, Zhu J, Chen J, Chi R (2017b) Removal of Congo red from aqueous solution by adsorption onto different amine compounds modified sugarcane bagasse. Clean Techn Environ Policy 19(2):517–525

Yuh-Shan H, Gordon M (1999) Pseudo-second order model for sorption processes. Process Biochem 34(5):451–465

Zheng X, Dou J, Yuan J, Qin W, Hong X, Ding A (2017) Removal of Cs^+ from water and soil by ammonium-pillared montmorillonite/Fe_3O_4 composite. J Environ Sci 56:12–24

Zong Y, Zhang Y, Lin X, Ye D, Luo X, Wang J (2017) Preparation of a novel microsphere adsorbent of Prussian blue capsulated in carboxymethyl cellulose sodium for Cs (I) removal from contaminated water. J Radioanal Nucl Chem 311(3):1577–1591